SCIENTIFIC REPORTS

OPEN

SUBJECT AREAS:
SUPERCONDUCTING PROPERTIES AND MATERIALS
SUPERCONDUCTING DEVICES
ELECTRONIC PROPERTIES AND MATERIALS
NANOWIRES

Received
2 May 2013

Accepted
12 July 2013

Published
29 July 2013

Correspondence and requests for materials should be addressed to J.W. (jianwangphysics@pku.edu.cn) or M.H.W.C. (chan@phys.psu.edu)

Voltage-current properties of superconducting amorphous tungsten nanostrips

Yi Sun[1], Jian Wang[1,2], Weiwei Zhao[2], Mingliang Tian[2,3], Meenakshi Singh[2] & Moses H. W. Chan[2]

[1]International Center for Quantum Materials, School of Physics, Peking University, Beijing 100871, People's Republic of China, [2]The Center for Nanoscale Science and Department of Physics, The Pennsylvania State University, University Park, Pennsylvania 16802-6300, USA, [3]High Magnetic Field Laboratory, Chinese Academy of Sciences, Hefei 230031, Anhui, People's Republic of China.

The voltage-current (V-I) characteristics of tungsten (W) strips patterned by focused-ion-beam assisted deposition were studied at different temperatures and various magnetic fields applied perpendicular to the strips. At fields of 1 Tesla (T) and 2 T, a scaling behavior was observed in V-I isotherms, which can be fitted by quasi-three-dimensional (quasi-3D) vortex-glass (VG) to liquid transition theory.

The existence of vortices in the mixed state of a superconductor is one of the most fascinating research topics in superconducting physics[1–16]. The vortices can form liquid, crystalline, and glassy phases. The discovery of high critical temperature (T_C) superconductors (HTS) has made the detailed study of vortex phases possible because of the large anisotropy and thermal fluctuations in HTS systems[1–7]. In the presence of strong disorder, the zero resistance state corresponds to a vortex glass (VG) phase and with increasing temperature the transition to the vortex liquid phase induces a dissipative state[2,17]. This transition has been demonstrated by transport measurement in HTS systems like $YBa_2Cu_3O_7$ (YBCO)[1,3], $Pr_{2-x}Ce_xCuO_{4-y}$ (PCCO)[7] and $Bi_2Sr_{2-x}La_xCuO_{6+\delta}$ (BSLCO)[4,6]. However, VG transition-like behavior in conventional low critical temperature superconductors (LTS) has only been observed in very few systems, like Nb[8–10], In[11], and Mo_3Si[13] films.

In the last few decades, a technique – focused ion beam induced deposition (IBID) has been developed and successfully used to fabricate low dimensional superconducting materials including W[18–23]. The reported T_C of amorphous W-based nanostructures fabricated by IBID is around 5.2 K[18], which is much higher than that of single-crystal bulk W (12 mK)[24]. This synthesis technique and the associated increase in T_C makes it possible to observe different vortex states in mesoscopic W system. In two dimensional W systems fabricated by IBID, the direct observation of vortex melting utilizing scanning tunneling microscopy/spectroscopy (STM/STS) has been reported[25]. We report here a systematic study of V-I properties of W nanostructures.

In this paper, W strips with different dimensions are fabricated using a focused ion beam-chemical vapor deposition (FIB-CVD) system. Experimental studies of electronic transport properties, especially the V-I curve measurement of individual W strips at various temperatures and magnetic fields are reported. Under zero magnetic field, the strip jumps from superconducting to normal state directly as the current is increased to a temperature dependent critical value. Under a finite magnetic field at temperatures below a specific value T_g, the jump to the high resistance state is preceded by a state of low residual resistance. The size of the jump in the V-I curve decreases with increasing temperature and vanishes as T approaches T_g. For $T > T_g$, the V-I curves are continuous resembling a sigmoid function with a maximum curvature that decreases with increasing temperature. When plotted in *log-log* scale, the V-I curve at $T = T_g$ shows a power law dependence. Curves at $T > T_g$ show a concave curvature with increasing I and curves measured at $T < T_g$ prior to the jump show a convex curvature. This evolution in the shape of the V-I curves is similar to that found in HTS and type II superconducting films mentioned above, which has been explained by VG transition theory.

Results

A commercial FIB etching and deposition system (FIB/SEM FEI Quanta 200 3D) utilizing a beam of 30 keV singly-charged Ga^+ ions was used for sample synthesis. The substrate used was a lightly p-doped Si wafer with a 1 μm thick Si_3N_4 insulating layer on the surface. Tungsten hexacarbonyl [$W(CO)_6$] gas was injected on the sample surface near the focused beam scanned area through a needle nozzle. The ion beam was then scanned over

the sample surface in the designed pattern, depositing the non-volatile component of the precursor on the surface. The volatile component was removed and the base pressure before introducing the $W(CO)_6$ gas was lower than 1×10^{-5} Torr.

During deposition the system pressure was in the range of $\sim 10^{-5}$ Torr. Lateral nanostrips with various lengths, widths and thicknesses were deposited by a 30 pA ion-beam current onto the substrate. Changing the ion-beam current or the volume per dose can change the superconducting properties of the resulting W strips. The sample W strips were connected to large Pt contact pads, which serve as electrodes for four-terminal transport measurements, with four W strips whose deposition parameters were the same as that of the sample. The normal Pt electrodes were also synthesized using the IBID technique. A scanning electron micrograph (SEM) of a W nanostrip with 4 connecting W strips can be seen in the inset of Figure 1(a). The volume per dose used in deposition is 6.8×10^{-1} μm^3/nC for samples 1 and 3, and 3.4×10^{-1} μm^3/nC for sample 2. The length, width and thickness of the samples were measured by a scanning electron microscope. Transport measurements were carried out in a physical property measurement system (PPMS-Quantum Design). The data from three samples are shown in this paper. The sample dimensions are 1.43 μm long, 250 nm wide and 50 nm thick (sample 1); 3.2 μm long, 250 nm wide and 50 nm thick (sample 2) and 3.5 μm long, 200 nm wide and 30 nm thick (sample 3). The thickness of a similarly deposited W strip was measured by first cutting the strip with ion beam and then examined in a SEM chamber at a tilted angle. We estimate the uncertainty in the thickness to be no more than 5 nm. The elemental concentrations of our nanostrips detected by energy dispersive spectrum (EDS) are about 40%, 40%, and 20%, for W, C, and Ga, respectively, which is consistent with the value detected by electron probe microanalysis (EPMA)[18].

An SEM image of sample 1 is shown in the inset of Figure 1(a). The length of the sample is defined as the distance L between the inner edges of the two voltage electrodes. Figure 1(a) shows resistance as a function of temperature (*R-T*) for sample 1 at an excitation current of 50 nA in the temperature range of 2–300 K at zero magnetic field (*H*). This sample exhibits a superconducting transition and zero residual resistance below $T_C \sim 4.8$ K. The sample does not show metallic behavior in the normal state and the resistance actually shows a 10% increase when it is cooled from 300 K to 8 K. This non-metallic behavior is likely a consequence of the presence of impurities such as carbon, Ga and oxides and also high density of defects in the amorphous W strips formed during the FIB-CVD fabrication process[18,23]. In order to study the superconductivity near or below T_C, the *R-T* curves in the low temperature regime (2 K ~ 6 K) are measured. Figure 1(b) shows *R-T* curves in the low-temperature regime measured at different *H*. In this paper, the applied magnetic fields are always perpendicular to the plane of the sample and substrate. The *R-T* curve of the W strip at zero field exhibits a superconducting transition at $T_C = 4.9$ K (onset T_C) and the width of the transition is about 0.2 K. On increasing *H*, the superconducting transition broadens and shifts to lower temperatures. Figure 1(c) shows the resistance of the W strip as a function of *H* at different temperatures. A superconducting transition with an onset critical field (H_{C2}) larger than 8 T at 2 K is seen. The H_{C2} of the strip decreases with increasing temperature. At a temperature of 6.0 K, the superconducting transition is barely noticeable.

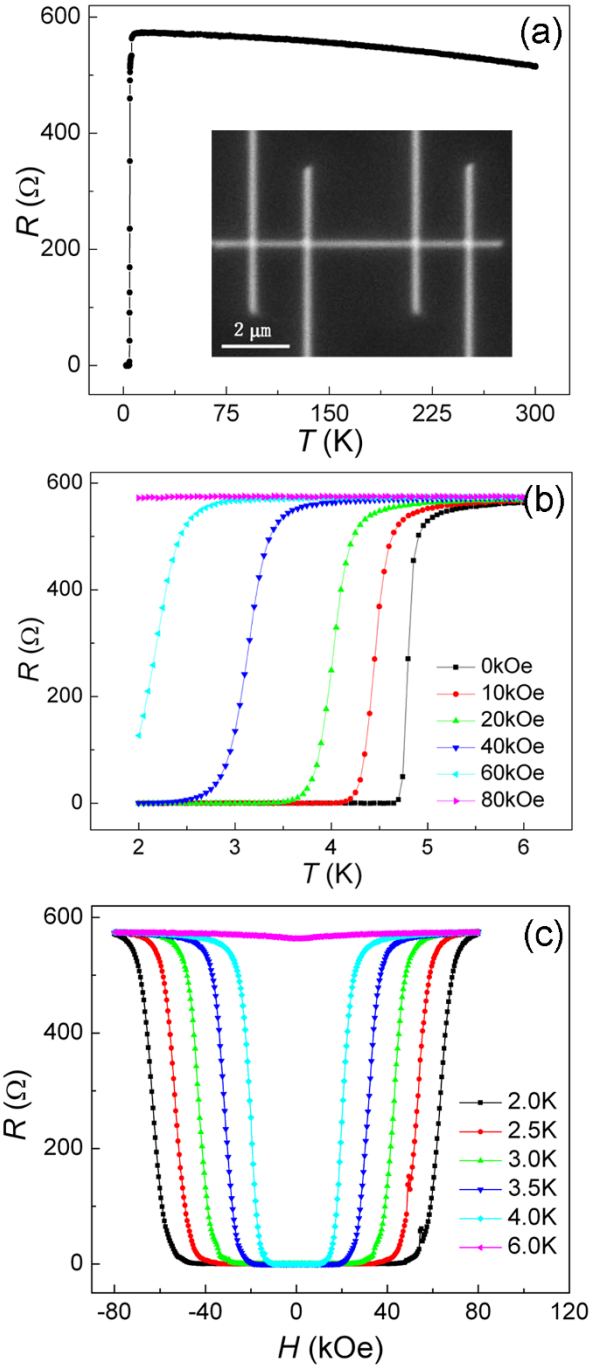

Figure 1 | Transport measurements of the W strip. (a) Resistance vs. temperature of W strip (sample 1). Inset is the SEM image of the sample with 4 connecting W electrodes; (b) Resistance vs. temperature of the W strip in different magnetic fields applied perpendicular to the plane of the sample; (c) Magnetoresistance of the sample at different temperatures.

Discussion

Although bulk W is a type I superconductor, the W strips measured in these experiments can be thought of as a type II conventional superconductor due to its finite thickness and amorphous structure with high density of defects as seen in transmission electron microscope (TEM) studies[23]. The disorders and defects act as pinning centers for vortices. For type II conventional superconductor Nb[8–10], the electric field – current density (*E-J*) isotherms measured at various temperatures at a given field value show qualitatively different behavior demarcated by a VG transition temperature, T_g. Near T_g, the curves show a power law relationship. For $T > T_g$, the *E-J* curves exhibit ohmic behavior and the resistivity remains constant at low currents. For $T < T_g$, $E \sim exp(-J/J^{\mu})$ resulting in a convex curvature in the *E-J* curves which is a signature of the vortex glass phase[6].

According to the VG transition theory[6], the *V-I* curves at different temperatures near T_g can be scaled into two different branches by the scaling law,

$$V\Big/I(T-T_g)^{\upsilon(z+2-D)}=A_{\pm}\left(I\Big/|T-T_g|^{\upsilon(D-1)}\right) \quad (1)$$

where υ is the exponent of the coherence length ξ, $\xi\sim|T-T_g|^{-\upsilon}$, and z is the dynamical exponent of the coherent time ξ^z respectively, D is the dimension of the system, and $A_{\pm}$ are the scaling functions above and below T_g. In the vortex liquid phase for the temperature above T_g, the linear resistivity ρ_{lin} at low current behaves as,

$$\rho_{lin}\propto(T-T_g)^{\upsilon(z+2-D)} \quad (2)$$

The *V-I* isotherm at T_g should satisfy the power law,

$$V(I)|_{T-T_g}\propto I^{\alpha} \quad (3)$$

with $\alpha=(z+1)/(D-1)$. Previous theoretical and experimental studies show that $z=4\sim7$ and $\upsilon=1\sim2$ are reasonable values for a 3D VG phase transition[1,6,7,9]. In recent years, quasi-2D VG transitions have been reported, and the ranges of z and υ are similar to those for 3D[12].

The *V-I* curves of the W strips are obtained at various magnetic fields and different temperatures. In this paper, we have measured the *V-I* curves by ramping the current from low to high and from high to low values. Identical results are found and we report only the curves collected when the current is being scanned downward. Figures 2(a)–2(c) show *V-I* curves measured between 2 and 6 K at applied fields of 0 *Oe*, 10 *kOe* and 20 *kOe* respectively. At zero field, the measured voltage jumps abruptly from zero to the normal state value at well-defined temperature dependent critical current. However, at a field of 10 *kOe* (Figure 2(b)), at temperature below T_g, *V* first increases slowly with *I*. This is followed by an abrupt jump and then a more gradual increase with further increase in *I* towards

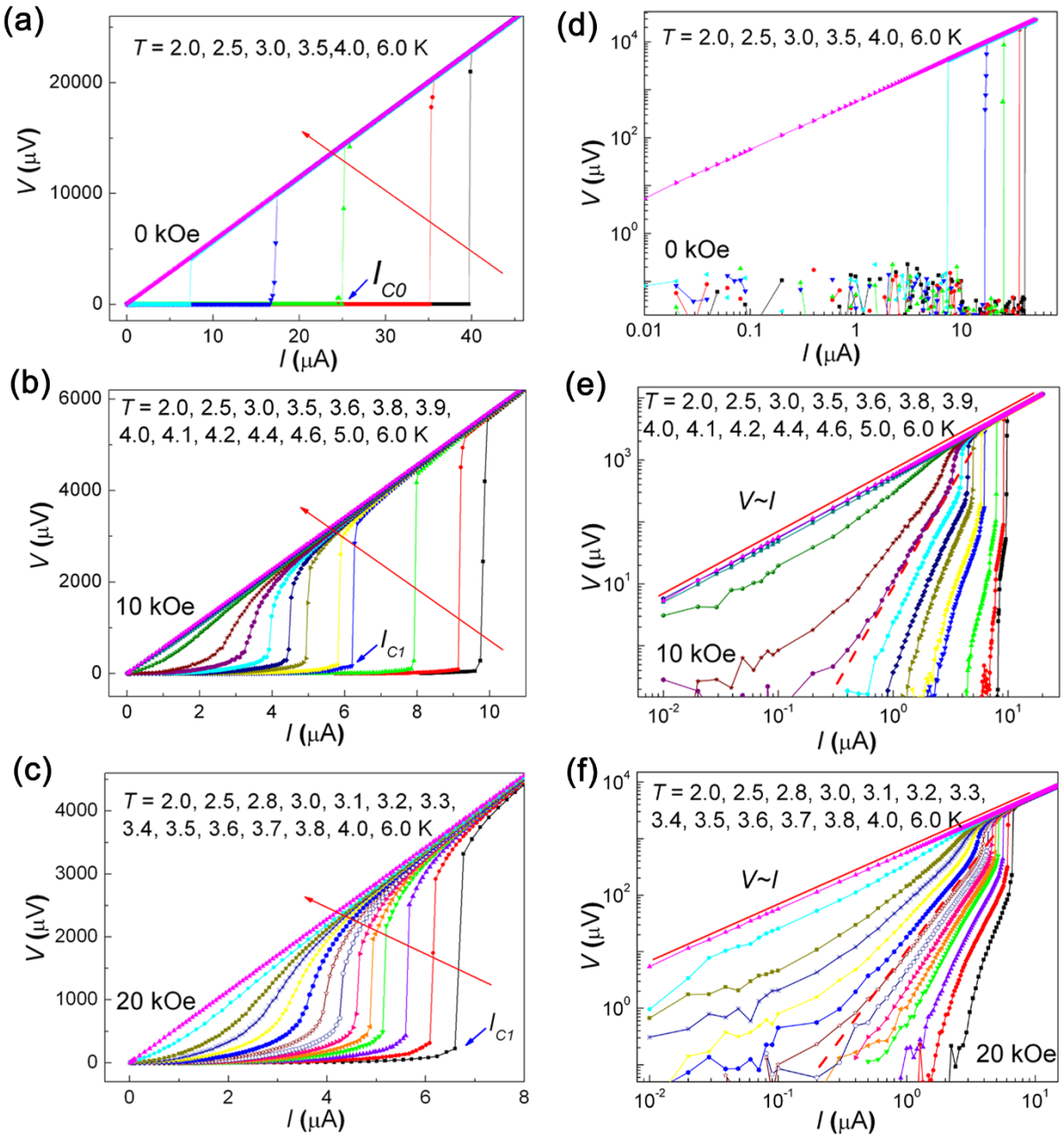

Figure 2 | *V-I* measurement of the W strip at different temperature and under magnetic field. (a–c) *V-I* characteristics measured at temperatures ranging from 2 to 6 K for H = 0 *kOe*, 10 *kOe* and 20 *kOe*, respectively. The red arrow points out that the measurement temperature changes from 2.0 K to 6.0 K. (d–f) *V-I* characteristics in *log-log* scales The dashed lines in panels (e) and (f) highlight power law *V-I* dependence at $T = T_g$ (4.05 K for measurements taken at 10 *kOe* and 3.4 K at 20 *kOe*).

ohmic behavior. *V-I* curves measured at $T > T_g$ do not show an abrupt jump and the curves are continuous resembling a sigmoid function. The maximum curvature of these curves decreases with increasing temperature. Similar evolution of *V* as a function of the current is seen at a field of 20 *kOe* (Figure 2(c)). The value of T_g decreases with magnetic field. The *V-I* curves shown in Figures 2(b) and 2(c) show that T_g at 10 *kOe* is near 4.0 K and at 20 *kOe* is near 3.4 K. We will show below that T_g can be more precisely identified by a more quantitative procedure. We define the critical current I_{C0}, where the voltage changes from zero to non-zero and critical current I_{C1}, where the voltage jumps rapidly.

The *V* vs. *I* dependence at low current is revealed in more details in *log-log* plots. Figure 2(d) clearly shows that at zero field the *V-I* curves show an abrupt change from the superconducting to the normal ohmic behavior at well defined I_Cs for all $T < T_C$. For measurements at fields of 10 and 20 *kOe*, the *log V - log I* curves (Figures 2(e) and 2(f)) at currents smaller than I_{C1} show a smooth evolution in the curvature from being convex to concave with increasing temperature. The curves with different curvature are separated by a curve showing power law dependence measured at or near $T = T_g$. This behavior is reminiscent of the vortex-glass state with the crossover temperature $T_{C\text{-}O}$ corresponding to the VG transition temperature - T_g. When the temperature is below T_g, and the sample is in the vortex glass state, the resistance falls rapidly with decreasing current and is zero below I_{C0}. At temperatures above T_g, the sample is in the vortex liquid state, the *V-I* curves exhibit ohmic behavior and the resistance remains constant even at small excitation currents. T_g can be more precisely identified by plotting the slope (*dV/dI*) as a function of *I* for each *T* numerically computed from the data of Figures 2(b) and 2(c). For $T < T_g$, the curves show a sharp and theoretically infinite *dV/dI* peak at some current, for $T > T_g$, the *dV/dI* shows a low and wide peak (shown in Figures 3(a) and 3(b)). After plotting the inverse of the maximum *dV/dI* values shown in insets of Figures 3(a) and 3(b) for each temperature (black line), the changing rate of the slope can be calculated as a function of temperature shown in blue line in the inset of Figures 3(a) and 3(b). The T_g of sample is the point which has the maximum changing rate of inversed maximum *dV/dI* value vs. *T* (4.05 K for the curves under a field of 10 *kOe* and 3.4 K for 20 *kOe*). A red dashed line in Figures 2(e) and 2(f) represents the *V-I* behavior at T_g. The fitted line satisfies the relation—$V \sim I^{\alpha}$ where α is 3.15 and 3.16 for Figures 2(e and 2(f)) respectively. The values at different fields are in close agreement.

The inset of Figure 4 shows the *log R-T* curve of sample 1 at 10 *kOe* with fit based on Eq. (2). The T_g value is 4.05 K. The slope of the fitting curve is $\upsilon(z+2-D)$. In order to get reasonable values of *z* and υ within the limits mentioned above ($z = 4 \sim 7$ and $\upsilon = 1 \sim 2$), the dimension *D* is taken to be 3 and the fitting parameter values are found to be $z = 5.31$ and $\upsilon = 0.99$. This means our W strip system shows quasi-3D behavior. This is reasonable since the coherence length of W strip is about 6 nm[17], which is much smaller than the thickness and width of the sample. Figure 4(a) shows the scaling collapse of the *V-I* isothermals according to Eq. (1) based on the experimental *V-I* curves at 10 *kOe* and the obtained parameter values

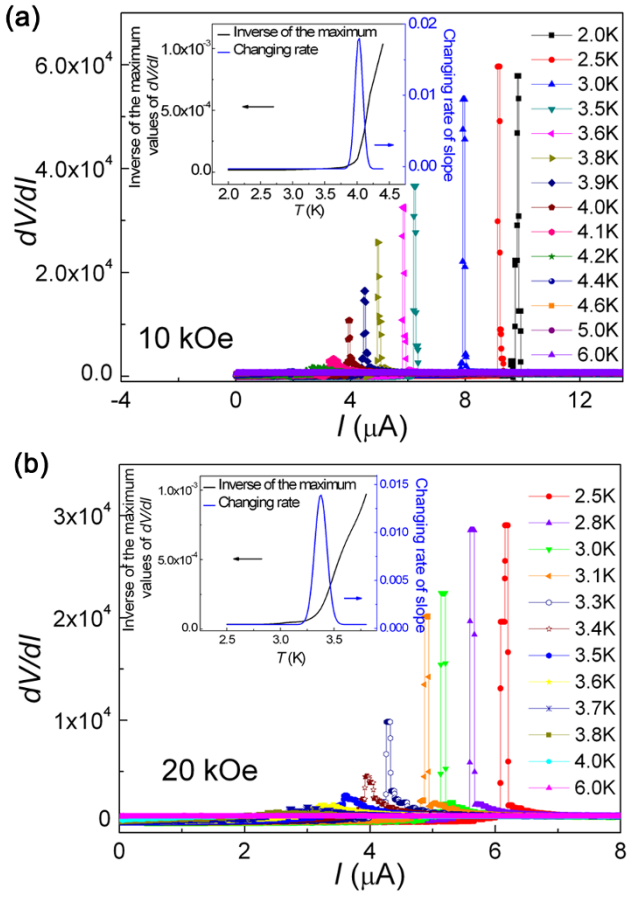

Figure 3 | *dV/dI-I* plots at temperatures ranging from 2 to 6 K for 10 *kOe* and 20 *kOe*, respectively. The insets show the inverse of the maximum values of *dV/dI* (black line) and the changing rate of the slope of the black line. The blue line exhibits that the max changing rate is at 4.05 K and 3.4 K for 10 kOe and 20 kOe, respectively.

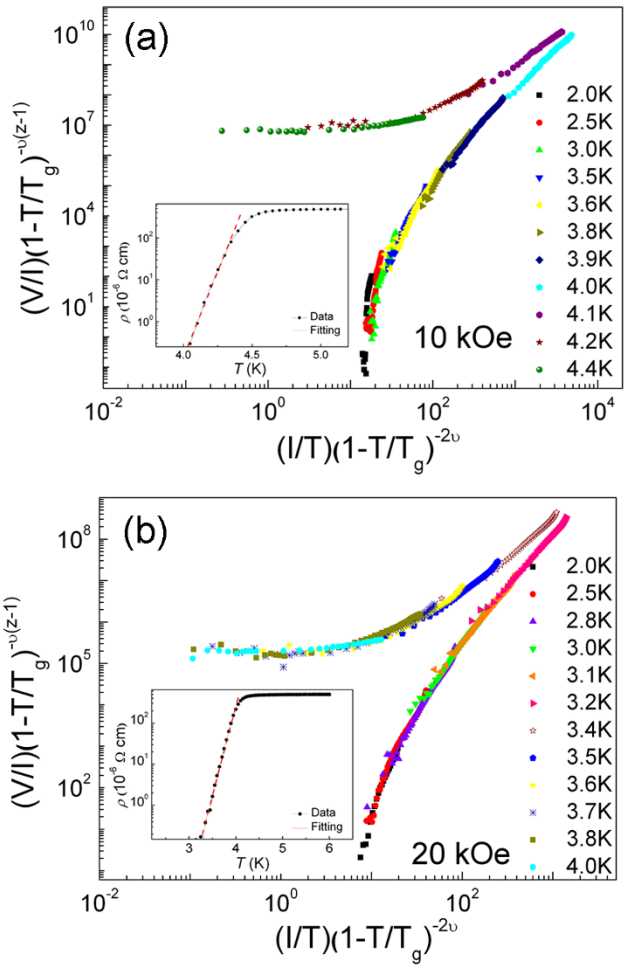

Figure 4 | Quasi-3D VG scaling of the *V-I* curves measured at 10 *kOe* and 20 *kOe* respectively. The insets show a logarithmic plot of the temperature dependence of the linear resistivity along with the fit used to obtain the scaling parameters.

($z = 5.31$and $\upsilon = 0.99$).The experimental *V-I* curves formed two universal branches corresponding to the data above and below T_g (4.05 K). Similar universal scaling behavior can be obtained for the *V-I* curves at a field of 20 *kOe* (Figure 4(b)) with parameter values of $T_g = 3.4K$, $z = 5.33$ and $\upsilon = 0.99$.

The *V-I* isothermals under different magnetic fields at 2 K (Figure 5(a)) are qualitatively similar to the *V-I* curves at different temperatures at fixed magnetic fields. The difference is that the *V-I* curves are separated into two parts by a particular field - H_g shown by a red dashed line in Figure 5(a). The isotherms are concave at the fields higher than H_g, while they are convex at fields lower than H_g. H_g plays the same role for these curves as T_g did in the discussion above. When the applied field is smaller than H_g, the voltage drops rapidly with decreasing current. At fields larger than H_g, the *V-I* curves exhibit ohmic behavior and the resistance remains constant in small current. This behavior exhibits the characteristics of a vortex glass-liquid transition. H_g can be considered to be the critical field of the VG phase transition. On the basis of the VG transition theory, the Eq. (1) can be rewritten in the following form:

$$V\Big/I(H-H_g)^{\upsilon(z+2-D)} = A_{\pm}\left(I\Big/\left|H-H_g\right|^{\upsilon(D-1)}\right) \qquad (4)$$

Utilizing Eq. (4) and an approach similar to the one described above (also see Supplementary Information), the related parameter values can be obtained ($H_g = 35$ *kOe*, $z = 7.07$ and $\upsilon = 0.89$), the *V-I* isothermals collapse onto two different branches as shown in Figure 5(b). The values of z and ν are a little deviation from the reasonable ranges mentioned above, which is possibly due to the limited thickness and width of the nanostrip.

Figure 6(a) is the *H-T* phase diagram for sample 1 (W strip). The values of the upper critical field H_{C2}, are extracted from the *R-H* curves at different temperatures shown in Figure 1(c). The fitting line in Figure 6(a) is based on the empirical temperature dependence of H_C (Eq. (5)).

$$H_{C2}(T) = H_{C2}(0)\left[1-\left(\frac{T}{T_C}\right)^2\right] \qquad (5)$$

In Figure 6(a), the black dots are T_g at 1 T and 2 T obtained from the *V-I* curves in Figure 3. The dashed fitting line is obtained using empirical formula (6)[17],

$$H_m(T) \sim \left(1-\frac{T}{T_C}\right)^{2\upsilon} \qquad (6)$$

$H_m(T)$ is the field corresponding to the vortex glass melting temperature (T_g). From the *V-I* data at different temperatures and under different magnetic fields (see Figures 2(e) & 2(d), Figure 5(a)), the value of T_g at 10 *kOe* and 20 *kOe*, H_g at 2 K can be derived. With two values of parameter ν obtained by fitting Eq. (2) earlier (0.99 and 0.89 under 10 *kOe* and 20 *kOe* field respectively), the fitting lines with two ν values are almost the same. We found that the data point - H_g at 2 K (the star mark) in Figure 6(a) lies on the red dashed fitting line which is the VG melting line. According to the phase diagram, each T_g corresponds a unique field along the transition curve. Thus, the H_g should be equivalent to T_g on the melting line.

According to Figure 2, the W strip is in totally superconducting state (zero voltage) below I_{C0}, then the voltage increases slowly till I_{C1}

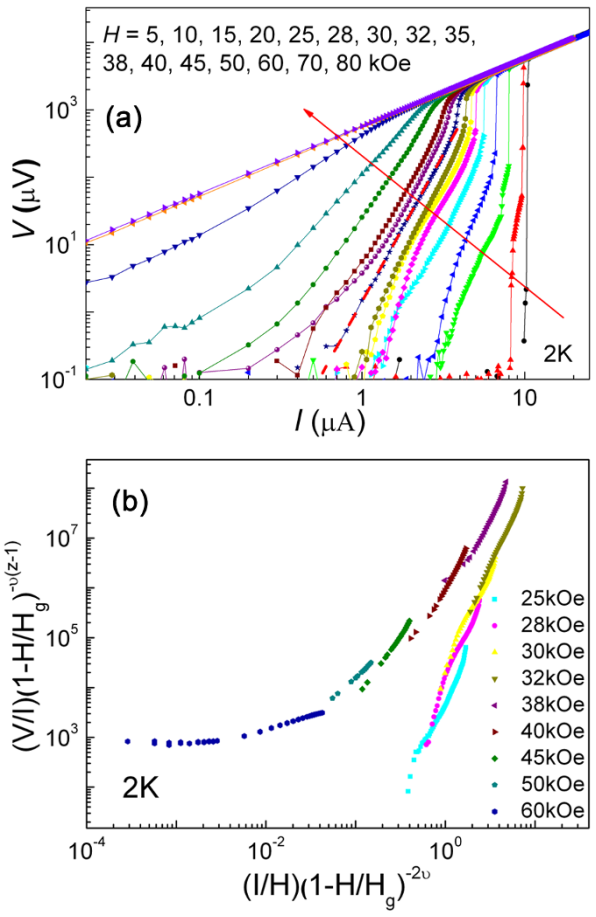

Figure 5 | *V-I* curves and Quasi-3D VG of the W strip at 2 K. (a) *V-I* characteristics measured at 2 K for magnetic fields ranging from 5 to 80 *kOe*; (b) Quasi-3D VG scaling of the *V-I* curves measured at 2 K.

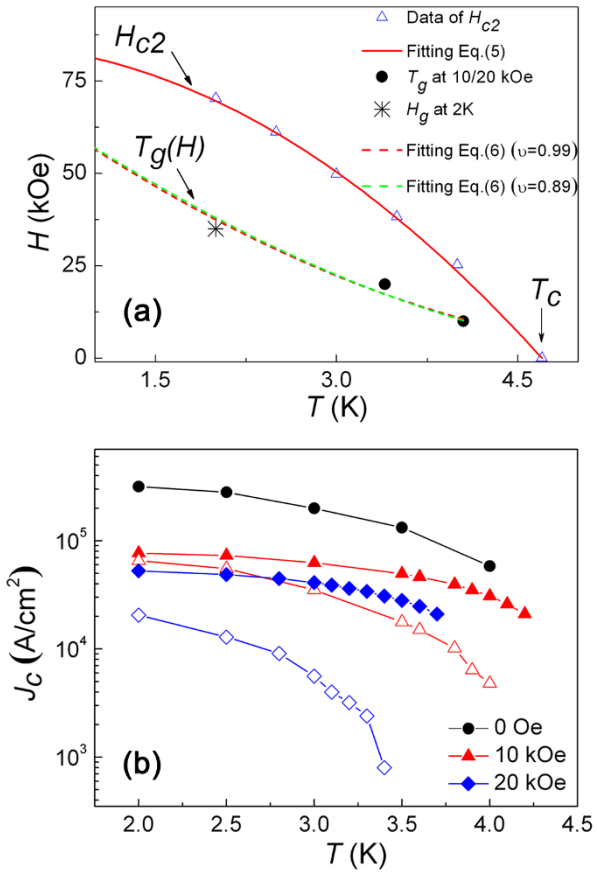

Figure 6 | The phase diagram and J_C varies with *T* of the W strip. (a) The phase diagram of magnetic field dependence of the melting temperature. (b) J_C calculated from I_C at various temperatures and perpendicular magnetic fields. J_{C0} is plotted by solid symbols and J_{C1} is drawn by open symbols. For 0 *Oe* data, the values of J_{C0} and J_{C1} are the same.

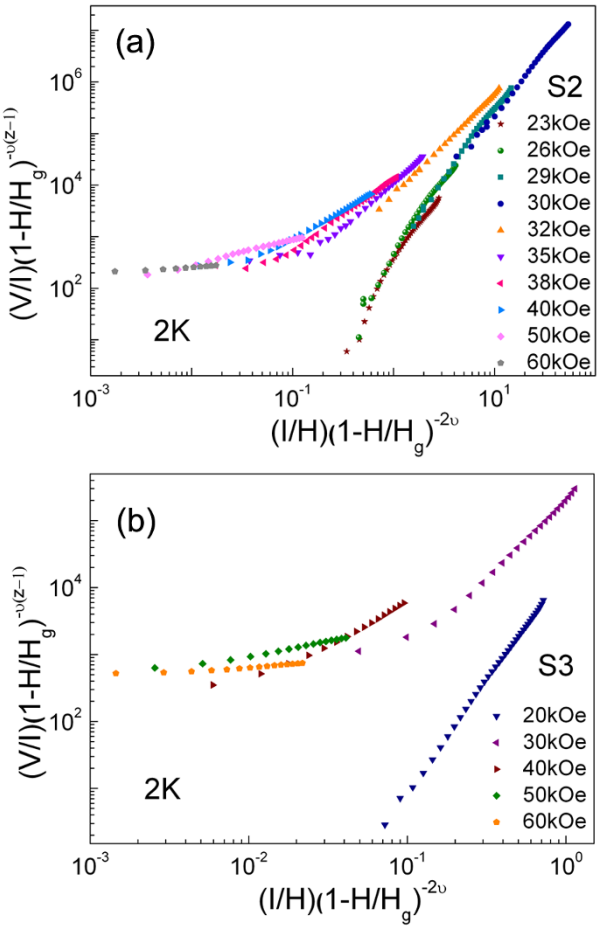

Figure 7 | Quasi-3D VG scaling of the *V-I* curves measured at 2 K for sample 2 and 3. (a) Quasi-3D VG scaling of the *V-I* curves measured at 2 K for sample 2; (b) Quasi-3D VG scaling of the *V-I* curves measured at 2 K for sample 3.

and jumps to the normal state. Figure 6(b) shows the critical current density J_{C0} and J_{C1}, calculated from I_{C0} and I_{C1} respectively, changing with temperature at 0, 10 and 20 *kOe*. The J_{C0} vs T curves obey the empirically parabolic law (Eq. (7)). For 0 Oe, the J_{C0} and J_{C1} are the same. The J_{C0} is $3.2\times10^5 A/cm^2$ at 2 K under 0 *Oe* field (The value in β - W film, of which T_C is 3.35 K, is about $10^6\sim10^7 A/cm^2$ [26]). With the temperature and magnetic field increasing, the values of J_C decreases.

$$I_{C\,i}(T) = I_{C\,i}(0)\left[1-\left(\frac{T}{T_C}\right)^2\right] \qquad (7)$$

The results discussed above were verified on the other two W strip samples by measuring their *V-I* characteristics at 2 K at different applied *H*. The crossover behavior (the curvature changes from convex to concave) discussed above was also observed in these samples at a particular field (H_g). In Figures 7(a) and 7(b), the *V-I* isothermals for samples 2 and 3 are scaling collapsed onto two branches obtained by using parameters: $H_g = 30.5$ *kOe*, $z = 5.24$ and $\upsilon = 0.67$ for sample 2, $H_g = 28$ *kOe*, $z = 6.02$ and $\upsilon = 0.53$ for sample 3. According to Figure 7, sample 2 obeys the VG scaling better than sample 3. This may be because that the thickness and width of sample 3 are distinctly smaller than those of sample 1 and sample 2. The small thickness and width limit the applicability of quasi-3D and quasi-2D VG transition theory to sample 3 and quasi-1D size effects may need to be taken into account in this situation.

In summary, the *V-I* curves of the W strips fabricated by focused ion beam & chemical vapor deposition are measured at different magnetic fields and temperatures. The scaling analysis of the *V-I* isothermals of W nanostrip (sample 1 and sample 2) follows the quasi-3D VG transition theory well. Every VG transition temperature T_g has a corresponding H_g along the VG melting line *i.e.* H_g appears to be equivalent to T_g in VG transition. However, the thinnest W strip (sample 3) shows a larger deviation from the conventional quasi-3D VG fitting. This may be because quasi-1D effects are not negligible in this situation[27] and have to be considered in future theoretical studies.

1. Koch, R. H. *et al.* Experimental evidence for vortex-glass superconductivity in Y-Ba-Cu-O. *Phys. Rev. Lett.* **63**, 1511 (1989).
2. Fisher, M. P. A. Vortex-glass superconductivity: A possible new phase in bulk high-T_C oxides. *Phys. Rev. Lett.* **62**, 1415 (1989).
3. Jiang, W. *et al.* Vortex-solid melting and depinning in superconducting Y-Ba-Cu-O single crystals irradiated by 3-MeV protons. *Phys. Rev. B* **47**, 8308 (1993).
4. Yarnasaki, H. *et al.* Quasi-two-dimensional vortex-glass transition observed in epitaxial $Bi_2Sr_2Ca_2Cu_3O_x$ thin films. *Phys. Rev. B* **50**, 12959 (1994).
5. Zhang, Y. Q. *et al.* Effect of stripe order on the vortex phase transition in $La_{1.44}Nd_{0.4}Sr_{0.16}CuO_4$ films. *Supercond. Sci. Technol.* **22**, 085010 (2009).
6. Zhang, Y. Z. *et al.* Vortex characteristics in a superconducting $Bi_2Sr_{2-x}La_xCuO_{6+\delta}$ thin film. *Phys. Rev. B* **62**, 11373 (2000).
7. Sullivan, M. C. *et al.* Scaling analysis of the static and dynamic critical exponents in underdoped, overdoped, and optimally doped $Pr_{2-x}Ce_xCuO_{4-y}$ films. *Phys. Rev. B* **81**, 134502 (2010).
8. Ando, Y., Kubota, H. & Tanaka, S. Observation of a vortex-glass phase in a narrow strip of Nb. *Phys. Rev. B* **48**, 7716 (1993).
9. Villegas, J. E. *et al.* Vortex phases in superconducting Nb thin films with periodic pinning. *Phys. Rev. B* **72**, 174512 (2005).
10. Villegas, J. E. & Vicent, J. L. Vortex-glass transitions in low-T_C superconducting Nb thin films and Nb/Cu superlattices. *Phys. Rev. B* **71**, 144522 (2005).
11. Okuma, S. & Kokubo, N. Universal critical scaling of dc and ac complex resistivities in an indium film near the vortex-glass transition. *Phys. Rev. B* **56**, 14138 (1997).
12. Yang, H. *et al. I-V* characteristics of the vortex state in MgB_2 thin films. *Phys. Rev. B* **76**, 134513 (2007).
13. Yeh, N.-C. *et al.* Universality, critical dynamics, and vortex diffusion in amorphous Mo_3Si films and $YBa_2Cu_3O_7$ single crystals. *Phys. Rev. Lett.* **71**, 4043 (1993).
14. Ning, Y. X. *et al.* Vortex properties of two-dimensional superconducting Pb films. *J. Phys.: Condens. Matter* **22**, 065701 (2010).
15. Xiao, Z. L. *et al.* Observation of the vortex Lattice spinodal in $NbSe_2$. *Phys. Rev. Lett.* **92**, 227004 (2004).
16. Lee, H. S., Bartkowiak, M., Kim, J. S. & Lee, H.-J. Magnetic-field-induced crossover of vortex-line coupling in $SmFeAsO_{0.85}$ single crystal. *Phys. Rev. B* **82**, 104523 (2010).
17. Fisher, D. S., Fisher, M. P. A. & Huse, D. A. Thermal fluctuations, quenched disorder, phase transitions, and transport in type-II superconductors. *Phys. Rev. B* **43**, 130 (1991).
18. Sadki, E., Ooi, S. & Hirata, K. Focused-ion-beam-induced deposition of superconducting nanowires. *Appl. Phys. Lett.* **85**, 6206 (2004).
19. Jenkins, D. W. K., Allen, G. C., Prewett, P. D. & Heard, P. J. Focused ion-beam assisted deposition of tungsten and carbon. *J. Phys.: Condens. Matter* **3**, S199 (1991).
20. Langfischer, H., Basnar, B., Hutter, H. & Bertagnoli, E. Evolution of tungsten film deposition induced by focused ion beam. *J. Vac. Sci. Technol. A* **20**, 1408 (2002).
21. Gross, M. E., Harriott, L. R. & Opila, R. L. Focused ion beam stimulated deposition of aluminum from trialkylamine alanes. *J. Appl. Phys.* **68**, 4820 (1990).
22. Horváth, E. *et al.* Morphological and electrical study of FIB deposited amorphous W nanowires. *Microelectronic Engineering* **84**, 837 (2007).
23. Li, W. X. *et al.* Tunability of the superconductivity of tungsten films grown by focused-ion-beam direct writing. *J. Appl. Phys.* **104**, 093913 (2008).
24. Gibson, J. W. & Hein, R. A. Superconductivity of Tungsten. *Phys. Rev. Lett.* **12**, 688 (1964).
25. Guillamón, I. *et al.* Direct observation of melting in a two-dimensional superconducting vortex lattice. *Nature Phys.* **5**, 651 (2009).
26. Bond, W. L. *et al.* Superconductivity in films of β-tungsten and other transition metals. *Phys. Rev. Lett.* **15**, 260 (1965).
27. Arutyunov, K. Y., Golubev, D. S. & Zaikin, A. D. Superconductivity in one dimension. *Phys. Rep.* **464**, 1 (2008).

Acknowledgments

We acknowledge Yuan Li and Xincheng Xie for fruitful discussions. This work was financially supported by National Basic Research Program of China (Grant Nos. 2013CB934600 & 2012CB921300), the National Natural Science Foundation of China (Nos. 11222434, 11174007 & 11174294), National Key Basic Research of China (Grant Nos.

2011CBA00111), the Pennsylvania State University Materials Research Science and Engineering Center under National Science Foundation Grant No. DMR-0820404, and China Postdoctoral Science Foundation (No. 2011M500180 & No. 2012T50012).

Author contributions

J.W. conceived and designed the study. J.W. and W.Z. did the experiments. M.T. and M.C. gave scientific advice. Y.S. analyzed the data. Y.S. and J.W. wrote the manuscript. M.C., M.S. and M.T. contributed to the discussion and revised the manuscript.

Additional information

Supplementary information accompanies this paper at http://www.nature.com/scientificreports

Competing financial interests: The authors declare no competing financial interests.

How to cite this article: Sun, Y. *et al.* Voltage-current properties of superconducting amorphous tungsten nanostrips. *Sci. Rep.* **3**, 2307; DOI:10.1038/srep02307 (2013).